VIII. FUELING

W. A. HOULBERG (ORNL)

Peaked density profiles may not only improve confinement properties, but also give the additional benefits of increased fusion production and ignition margin in BPX, as shown in Fig. 8.1. The ability to control density profiles in the core and scrape-off regions is governed by a number of both physics and operational considerations that make it difficult to specify optimized fueling systems. For this reason, the fueling systems for BPX are designed to maximize flexibility, allowing operation to determine optimal scenarios. After listing some of the issues impacting fueling assessments, we present the latest information on pellet ablation and penetration and then give example fueling scenarios.

Some degree of external control over the density profile in the core can be achieved through pellet injection, but recycle and other plasma edge physics limit the degree of control that is possible. Passive pumping and fueling by the walls, limiters, and other structures (collectively called fuel recycle) is a function of the temperature of the surface, incident particle energy, and history of the fluence.[1] In H-mode operation, diffusive losses are sharply reduced at the separatrix, and the lower scrape-off density allows better penetration of neutrals released from the structures; together these lead to an increase in the plasma particle content and can lead to very broad or even hollow density profiles in the core. The high operating plasma density in BPX, however, and active wall conditioning techniques, may amelioriate these effects relative to present devices.

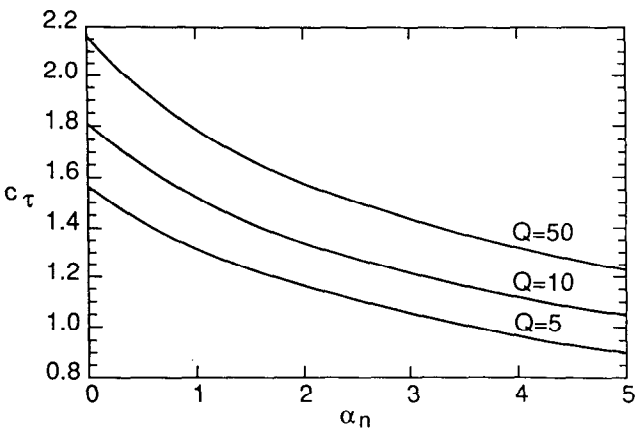

Fig. 8.1. The required confinement enhancement factor C_τ (relative to $\tau_{ITER89-P}$) to reach a given Q value decreases with increased density profile peaking characterized by α_n. The density profile is given by $n(r) = n(0)(1 - r^2/a^2)^{\alpha_n}$. Plasma conditions are $Z_{eff} = 1.65$ (carbon), $n_\alpha/n_e = 0.03$, $n_D = n_T$, and $T_e = T_i$.

The plasma edge density almost certainly influences density limits, L-H transitions, neutral gas penetration and fueling efficiency, the resistive load on radio-frequency (RF) antennas, and—of critical importance in assessing power handling—the average energy of particles striking the divertor plates, walls, and other edge structures. The scrape-off density is governed by pumping in the divertor region and recycle from walls and other structures as well as external gas feed. An assessment of fueling needs must then be closely coordinated with an evaluation of active and passive pumping (see Chap. IX).

Maximum fueling rates are typically dictated by maximum desired density ramp rates during startup, whereas maximum pumping rates are determined by how fast density needs to be ramped down to avoid disruptive density limits as the plasma temperature, toroidal field, and current are reduced at the end of the discharge. Raising the average density by 3×10^{20} m^{-3} over a 5-s interval requires a net source of 4×10^{21} (D + T) s^{-1}. This dictates a minimum pellet frequency for pellets of a given size: 1 Hz for pellets of effective spherical radius $r_p = 2.5$ mm or 2 Hz for $r_p = 2$ mm. Allowing for faster ramp rates and some net pumping by material surfaces dictates that the pellet injection system be designed to operate at two to three times this fueling rate. The net pumping required during rampdown can be calculated in a similar manner; reducing the density by 3×10^{20} m^{-3} over a 10-s rampdown requires a minimum net pumping rate of 2×10^{21} s^{-1}. Allowing for the possibility of a net source from material surfaces (e.g., outgassing because of elevated temperatures at the end of the burn) and faster pumpdown rates dictates that the BPX design should handle at least twice this pumping rate. In the flattop phase, auxiliary fueling and net pumping must balance.

To maximize the range of possible operating scenarios and conditions available to BPX, a very flexible fueling system is specified: The gas fueling system is augmented by a nominal 1.5 km/s pellet injector and an advanced 4 to 5 km/s in-

jector. The gas system is required for prefill and early startup as well as for control over scrape-off conditions during other phases of operation. It is possible to meet these gas fueling needs with a deuterium-only system, while reserving tritium fueling for the more efficient pellet injection systems. The 1.5 km/s pellet injector, based on modest extensions of present technology, provides central penetration during startup and ohmic conditions. When tritium fueling is delayed until the onset of RF heating, pellet injection provides the means of bringing the tritium density rapidly to the desired burn conditions. The 4 to 5 km/s pellet injector, requiring more technology development, allows for more aggressive density profile control and improved tritium fueling efficiency during burn.

VIII.A. PELLET PENETRATION

Extensive pellet data bases from JET and ASDEX have been used to evaluate the scaling of penetration with plasma density, electron temperature, pellet size, and velocity over a wide variety of plasma conditions.[2,3] The results of these experiments confirm the scaling derived from the neutral gas shielding model. The normalized pellet penetration depths (λ/a_o, where a_o is the distance from the magnetic axis to the limiter or separatrix) from pellet velocity experiments in JET ohmic plasmas are shown in Fig. 8.2, along with projections for BPX. Because there is an expected strong dependence of penetration on pellet size and plasma temperature, experimental variations in these parameters must be removed to uncover the weaker dependence on pellet velocity. This can be done either by tightly controlling the experimental conditions or by removing known parameter dependences analytically—both have been examined. The group of low-velocity ($v_p \approx 0.5$ km/s) JET cases clustered around $\lambda/a_o \approx 0.5$ correspond to essentially the same experimental conditions as the group of higher velocity ($v_p \approx 1.3$ km/s) JET cases around $\lambda/a_o \approx 0.7$, since these points were generated in pairs on sequential shots with the nominal 2.7-mm diameter and length cylindrical pellets. Other data points correspond to larger pellets or higher or lower temperature plasmas. Analytic removal of expected parameter dependences is shown in Fig. 8.3 where the velocity scale is normalized to the neutral gas shielding parameter:

$$C_p = \frac{n_m}{a_o}\left[\frac{A_{pel}}{n_e(0)}\right]^{1/3}\left[\frac{r_p}{T_e(0)}\right]^{5/3},$$

where n_m is the molecular density of the solid pellet ($n_m = 3.16 \times 10^{28}$ m^{-3} for a 50/50 D/T mix), A_{pel}

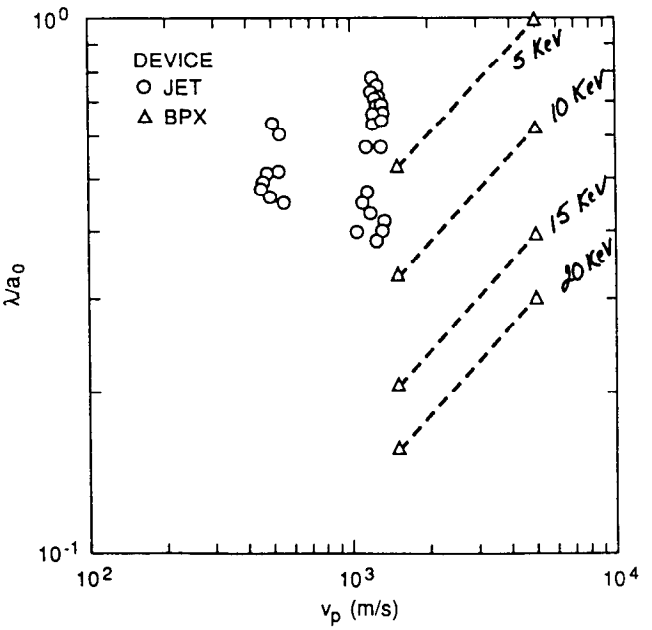

Fig. 8.2. Data from JET covers the ranges r_p = 1.12 to 2.41 mm, $T_e(0)$ = 1.63 to 4.11 keV, and $n_e(0)$ = 2.27 to 5.44 × 10^{19} m^{-3}, in addition to the velocity range shown. The BPX pellets are r_p = 2.0 mm at v_p = 1.5 km/s and r_p = 2.5 mm at v_p = 5 km/s, with penetration calculated from the scaled JET results.

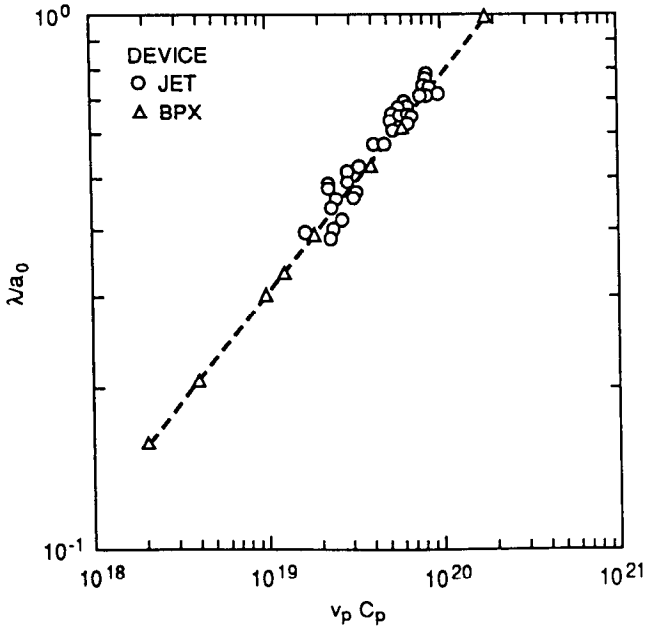

Fig. 8.3. The normalized pellet penetration from JET can be used to scale pellet penetration to BPX conditions using the neutral shielding parameter C_p.

is the mass number of the pellet species, r_p is the effective spherical pellet radius, and $n_e(0)$ and $T_e(0)$ are the central plasma electron density and temperature, respectively (all with units of SI-keV). The neutral gas shielding model predicts $\lambda/a_o \propto (C_p v_p)^\alpha$ with $\alpha = 1/3$ for parabolic profiles. The theory expects α to be dependent on profile shapes; this has been confirmed by ASDEX data.[3] The best fit to the JET data, $\alpha = 0.4$, was used for the BPX projections, giving $\lambda/a_o = 7.6 \times 10^{-9}(C_p v_p)^{0.4}$ for the empirical fit.

The high pellet ablation rates expected in high-temperature BPX plasmas may lead to an additional shielding phenomenon known as magnetic shielding, whereby the cold, high-beta plasma surrounding the pellet deflects the field lines around the pellet and reduces the effective incident electron energy flux. It is not known whether these very localized (≈1 cm), transient (≈10 μs) perturbations will cause any further plasma disturbances. The theory of magnetic shielding is being examined under the BPX Physics R&D plan. If magnetic shielding is found to be important for BPX, the penetration depths may be greater than projected from the present data base.

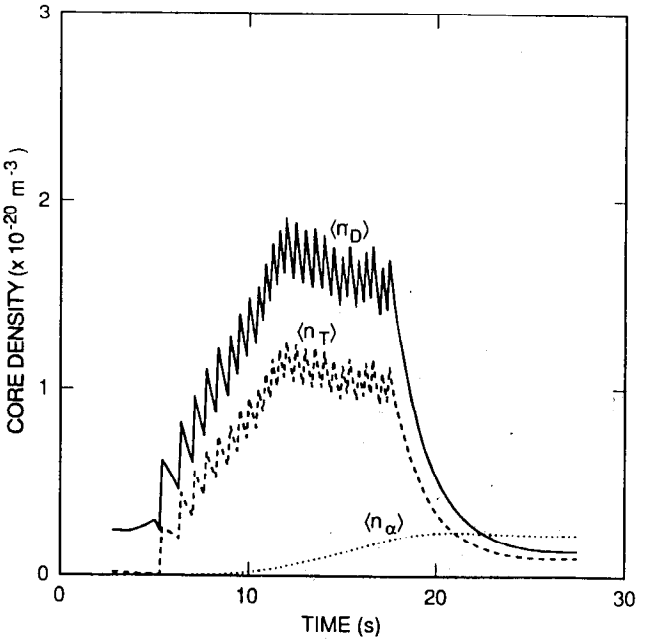

Fig. 8.4. The average tritium density in the core is lower than the deuterium density because of the 60/40 mixture of D-T assumed for the pellets (advanced injector: $v_p = 5$ km/s, $r_p = 2.5$ mm) in this tritium reduction case. Buildup of thermal helium is modest even with 100% recycle assumed.

VIII.B. FUELING SCENARIOS

The most efficient way of introducing tritium to the plasma is to wait until auxiliary heating begins, then inject tritium pellets. The breakdown and early current rise phases can consist of pure deuterium, plus appropriate minority components for RF heating. Examples of scenarios such as this have been run with the WHIST transport code, and a nominal ignited case is presented here for illustration.

The computational model consists of two-dimensional fixed boundary magnetohydrodynamic (MHD) equilibria from the VMOMS code[4] coupled with one-dimensional radial transport. The parallel losses in the scrape-off region are modeled as sink terms using the Emmert model.[5] Coronal equilibrium radiation losses are evaluated from Post et al.,[6] with $Z_{eff} \approx 1.65$ consisting of carbon, oxygen, and iron ($n_C/n_e = 0.0114$, $n_O/n_e = 0.001$, and $n_{Fe}/n_e = 0.00022$). Recycle of fuel particles from the walls and secondary limiters is assumed to be 100%, while recycle from the divertor plates is modeled as a reduction in the return charged-particle flux. Helium is recycled at 100% and builds up during the discharge. The example presented here illustrates 98% divertor return flux (for D-T fuel) with the remainder assumed to be pumped by codeposition. Transport in the core consists of neoclassical terms plus anomalous contributions to diffusivities, $\chi_i^{an} = \chi_e^{an} = 5D_j^{an}$, and a moderate anomalous particle pinch, $v_p = -0.5 D_j^{an} x/a_o^2$. The anomalous transport coefficient in the core is adjusted to yield $\tau_E \approx 2\tau_{ITER89-P}$ in the ignited case. The radial profiles of all diffusivities increase parabolically from the axis to the separatrix by a factor of 5. In the scrape-off layer, $\chi_{e\perp}^{an} = 2$ m/s and $\chi_{i\perp}^{an} = D_j^{an} = 0.67$ m/s, consistent with the model described in Chap. IX. No attempt was made to include an edge barrier to simulate H-mode behavior.

Figure 8.4 shows the evolution of the volume-averaged deuterium, tritium, and thermal alpha densities, where deuterium gas fueling is used for $t < 5$ s, followed by pellets consisting of a 60/40 D-T mixture for the density ramp and remainder of the discharge. The pellets ($r_p = 2.5$ mm, $N \approx 4 \times 10^{21}$) are injected at $v_p = 5$ km/s, corresponding to the advanced injector specifications. The toroidal field is ramped linearly from 5 to 9 T over the interval $0 < t < 7.5$ s, and the plasma current is ramped linearly from 3 to 11.8 MA over the same time interval. RF heating at 20 MW is applied over $5 < t < 12$ s including 0.5 s each for power rampup and rampdown (130 MJ total en-

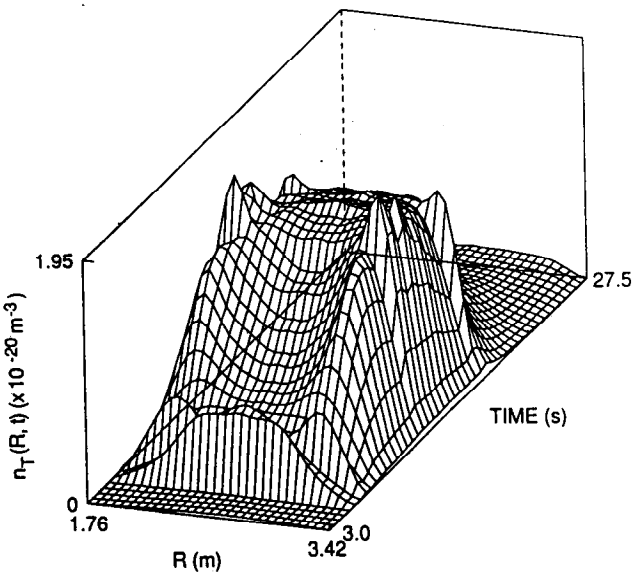

Fig. 8.5. The evolution of the tritium density profile shows initial penetration of the first pellet to the plasma center. Subsequent pellets during the density ramp and heating phase penetrate less deeply as evidenced by hollow density profiles during the strong ramp. Penetration is to about the edge of the sawtooth mixing region during the flattop phase, giving a peak-to-average density ratio of 1.5.

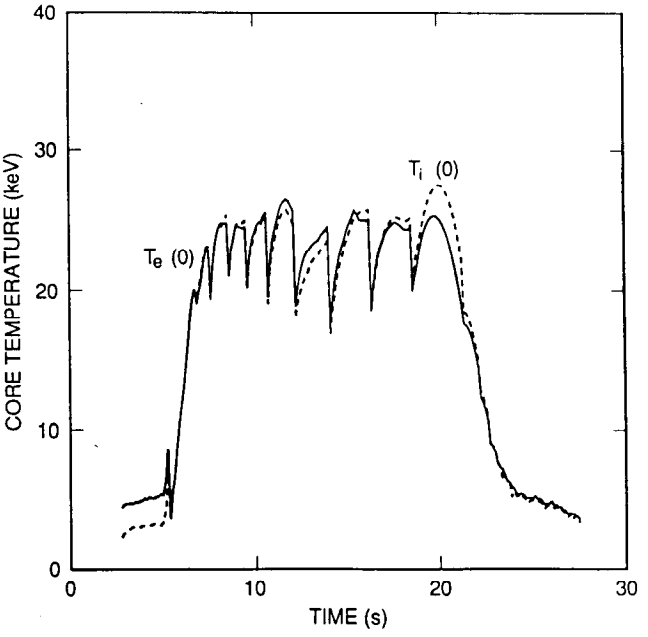

Fig. 8.6. Central electron and ion temperatures exhibit large fluctuations that are a consequence of the Kadomtsev sawtooth model.

ergy absorbed). The density rampdown begins at the end of the 10-s flattop phase ($7.5 < t < 17.5$ s) by turning off the pellet fueling. (The choice of timing in this simulation is not critical. No attempt is made to achieve consistency with divertor power handling constraints.) The helium (thermal alpha) concentration at the very end of the discharge is dominant because it is assumed that helium is not pumped during this interval. The toroidal field and and current are ramped down linearly over the interval $17.5 < t < 27.5$ s to 5 T and 3 MA at the end of the simulation.

The evolution of the tritium density profile (Fig. 8.5) shows that the first pellet penetrates to the center and instantly raises the tritium concentration throughout the plasma with a centrally peaked profile. As heating proceeds, the penetration is reduced, and the density profile is hollow during the remainder of the strong density ramp. During the flattop stage, sawtooth activity and pellet penetration to $r/a \approx 0.6$ (about the edge of the sawtooth mixing region) keep the central portion of the tritium density profile fairly flat. The deuterium and electron density profiles are similar to the tritium profile. During the burn phase, $\langle n_e \rangle_{core} \approx 3.3 \times 10^{20}$ m^{-3} and $n_e(0) \approx 5.0 \times 10^{20}$ m^{-3}, giving a peak-to-average value of 1.5. In a similar case, but without an anomalous particle pinch, the density profiles were somewhat broader and fusion power production was lower by about 30%, although the number of pellets required for fuel makeup was essentially the same as the base case.

The large-amplitude fluctuations in central electron and ion temperatures shown in Fig. 8.6 are a result of sawtooth activity using a Kadomtsev reconnection model. Fast alphas, thermal particles, and thermal energy are redistributed during the sawtooth crashes. The ion and electron temperature profiles are very similar because of strong coupling at these densities and temperatures. The plasma is ignited since it continues to burn after the auxiliary heating is turned off at 12 s, producing about 500 MW of fusion power. The plasma is de-ignited beginning at 17.5 s by turning off the auxiliary fueling and reducing the fuel density.

Evolution of the ion temperature profile projected onto the midplane is shown in Fig. 8.7. Other fixed boundary cases have been found with different B_T and I ramps in WHIST simulations that avoid sawtooth activity entirely (and maintain $q_o > 1.5$ throughout the entire flattop). This type of operation could be used to extend the high confinement results found with combined ICRF heating and pellet fueling in JET when $q_o > 1.5$ (Ref. 7). The Tokamak Simulation Code (TSC)

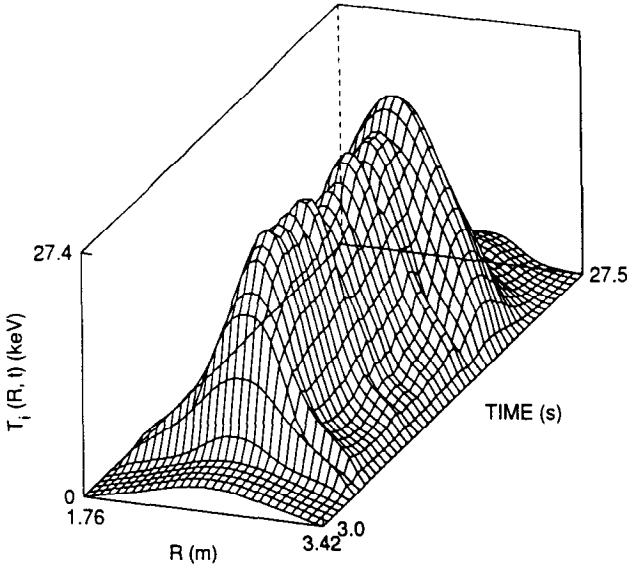

Fig. 8.7. The ion temperature profile is strongly peaked between sawteeth due to the strong central ICRF and alpha heating.

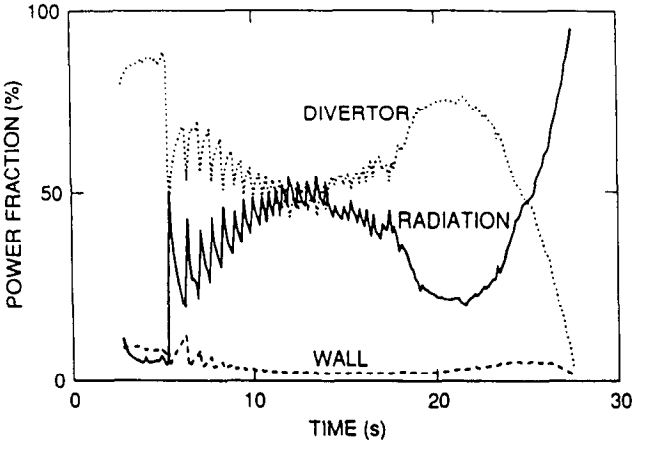

Fig. 8.8. The fractional power to the walls and limiters (by conduction, convection, and charge-exchange) is small while the remainder is split between radiation and flow to the divertor region.

runs using a full free-boundary MHD equilibrium model and poloidal field (PF) coil constraints have shown cases with small sawtooth inversion radii that would also allow more peaked density profiles.

The power fractions from radiation, flow to the divertor region, and charge-exchange and convection to the walls and secondary limiters (away from the divertor region), shown in Fig. 8.8, indicate that a density limit is reached at the very end of the simulation. (One manifestation of the density limit is when the radiative fraction reaches 100%.) Although these results are sensitive to the impurity mix, profile, radiation model (coronal equilibrium assumed here), and poloidal variations, they can be used as a guide in examining the flexibility of the fueling systems for separating control of core density from edge density and power flows. Power losses to the walls and secondary limiters are negligible throughout the discharge while radiation losses reach a maximum of 50%, with the remainder of the power flowing to the divertor region. When the density is lower during the initial portion of the density ramp, the pellets induce large fluctuations in the power flows. In a case that replaced pellet fueling by gas fueling during the density ramp, with all other aspects of the models and sequences the same, a radiative collapse, or density limit, was observed early in the ramp. The density at which this was observed was well below the expected density limit and may be due to inaccuracies in evaluating impurity radiation at low temperatures from the coronal equilibrium tables.[6]

A total of 25 pellets were injected in the long-burn-pulse case presented here. With $\approx 1.6 \times 10^{21}$ tritons per pellet ($\approx$ 80 Ci), this represents 2 kCi of tritium injected during the discharge. Operating with a 60/40 D-T pellet mixture has reduced tritium consumption by 20% from the nominal 50/50 D-T case without a significant sacrifice in fusion production. The reduction of tritium use by delaying injection until the heating phase is expected to be large but has not been quantified in these calculations because of the inability to reproduce the density ramp with gas makeup. Further reduction of tritium use is possible by introducing deuterium gas feed during the ramp and flattop phases (limited by density and radiation constraints). Deuterium gas feed lowers the scrape-off temperatures and the parallel particle flow velocity to the divertor region.

Evolution of the average electron and ion temperatures for a case with the smaller, lower velocity pellets (r_p = 2 mm, v_p = 1.5 km/s) is shown in Fig. 8.9. All other conditions are identical to the ignited case with the advanced injector. The shallower penetration of the lower velocity pellets does not produce ignition, and the discharge eventually terminates with a density limit disruption since fueling was continued after the temperature fell.

The assumption of 98% return flux from the divertor region leads to pumping in the range of 2 to 10×10^{21} s^{-1} for deuterium plus tritium, with the highest values during the flattop and early ramp-

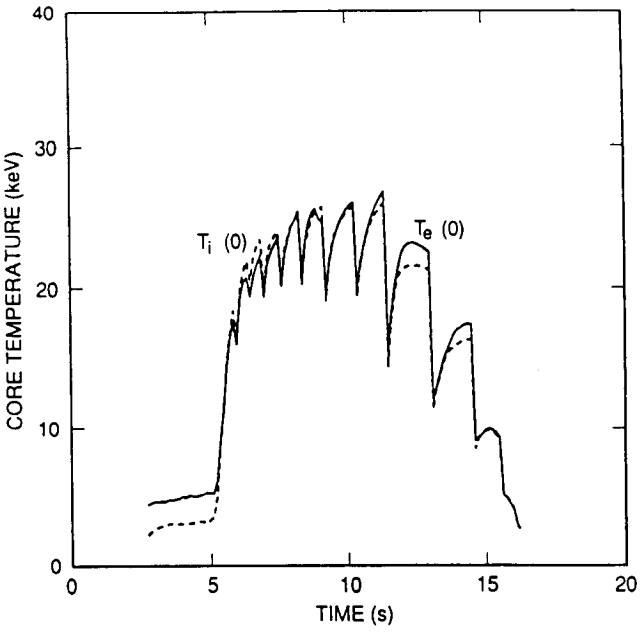

Fig. 8.9. With less deeply penetrating pellets ($v_p = 1.5$ km/s, $r_p = 2$ mm) the plasma quenches after auxiliary heating is terminated with all other conditions identical to the case presented in Figs. 8.6.

down phases. These values are somewhat high based on our present understanding of codeposition pumping in the divertor region (see Chap. IX) and need further refinement, but can be used as an upper limit on design of the fueling system. The fueling system consisting of gas feed, a nominal 1.5 km/s pellet injector and an advanced 5 km/s pellet injector—each capable of fueling up to 10^{22} particle/s of a D-T mixture—is flexible enough to cope with a large range of uncertainties while providing a measure of control over core and edge densities, tritium fueling efficiency, and power flows.

REFERENCES

1. P. C. STANGEBY and G. M. MCCRACKEN, "Plasma Boundary Phenomena in Tokamaks," *Nucl. Fusion,* **30,** 1225 (1990).

2. W. A. HOULBERG, "Pellet Ablation Results from JET," ITER Physics Report ITER-IL-PH-9-0-U-3, presented at ITER Workshop on Fueling, Garching, FRG, July 1990.

3. W. SANDMANN, "Model of a Simple Scaling Law in ASDEX," ITER Physics Report ITER-IL-PH-9-0-E-7, presented at ITER Workshop on Fueling, Garching, FRG, July 1990.

4. L. L. LAO, R. M. WIELAND, W. A. HOULBERG, and S. P. HIRSHMAN, "VMOMS – A Computer Code for Finding Moment Solutions to the Grad-Shafranov Equation," *Comput. Phys. Commun.,* **27,** 129 (1982).

5. G. A. EMMERT, R. M. WIELAND, A. T. MENSE, and J. N. DAVIDSON, "Electric Sheath and Presheath in a Collisionless, Finite Ion Temperature Plasma," *Phys. Fluids,* **30,** 803 (1980).

6. D. E. POST, R. V. JENSEN, C. B. TARTAR, W. H. GRASBERGER, and W. A. LOKKE, "Steady-State Radiative Cooling Rates for Low-Density, High-Temperature Plasma," *At. Data Nucl. Tables,* **20,** 397 (1977).

7. L. A. CHARLTON, L. R. BAYLOR, A. W. EDWARDS, G. W. HAMMETT, W. A. HOULBERG, P. KUPSCHUS, V. E. LYNCH, S. L. MILORA, J. O'ROURKE, and G. L. SCHMIDT, "Theoretical Analysis of the Role of the Infernal Mode in the Stability of Peaked Pressure Profiles in Pellet Fuelled JET Discharges," *Nucl. Fusion,* **31,** 1835 (1991).